

A LOCAL INFORMATION BASED VARIATIONAL MODEL FOR
SELECTIVE IMAGE SEGMENTATION*

JIANPING ZHANG

School of Mathematical Sciences, Dalian University of Technology
Dalian, Liaoning, 116024, ChinaKE CHEN¹Centre for Mathematical Imaging Techniques and Department of Mathematical Sciences
University of Liverpool, Liverpool L69 7ZL, United Kingdom

BO YU

School of Mathematical Sciences, Dalian University of Technology
Dalian, Liaoning, 116024, China

DEREK A. GOULD

Radiology Department, Royal Liverpool University Hospitals
Prescot Street, Liverpool L7 8XP, United Kingdom

(Communicated by Hao-Min Zhou)

ABSTRACT. Many effective models are available for segmentation of an image to extract *all* homogenous objects within it. For applications where segmentation of a *single* object identifiable by geometric constraints within an image is desired, much less work has been done for this purpose. This paper presents an improved selective segmentation model, without ‘balloon’ force, combining geometrical constraints and local image intensity information around zero level set, aiming to overcome the weakness of getting spurious solutions by Badshah and Chen’s model [8]. A key step in our new strategy is an adaptive local band selection algorithm. Numerical experiments show that the new model appears to be able to detect an object possessing highly complex and nonconvex features, and to produce desirable results in terms of segmentation quality and robustness.

1. Introduction. In the past two decades, image segmentation has been increasingly used because of rapid development in medical and satellite imaging among other applications. The goal of segmentation is to obtain a partition of a given image into a finite number of semantically important regions such as homogenous features or similar medical structures. A lot of competing approaches have been proposed to model image segmentation problems, including histogram analysis, region growing, edge detection and variational partial differential equation (PDE) methods based on optimizing energy functionals [6, 7, 8, 14, 18, 19, 22, 25, 28, 32, 34, 37, 44], and the research field is still much active.

2010 *Mathematics Subject Classification.* Primary: 62H35, 65N22, 65N55; Secondary: 74G65.

Key words and phrases. Active contours, local energy function, partial differential equations, segmentation, level sets, geometric constraints.

*This work is partially supported by the National Natural Science Foundation of China (11171051, 91230103) and the Royal Liverpool and Broadgreen University Hospitals NHS Trust of UK (85444/85446).

¹Corresponding author: <http://www.liv.ac.uk/cmit>, k.chen@liv.ac.uk

An early segmentation approach for computer vision is edge detection [5, 13, 38, 41] based on local properties of first or second order derivatives of image functions. Kass et al. [25] proposed the first energy minimizing functional for modelling image segmentation based on deforming a parameter curve towards the final solution curve defining edges of the detected objects. Although this classical ‘Snake’ deformation model was not robust and could not directly deal with changes in topology of the curves, it introduced the powerful variational theory of energy minimization and Euler-Lagrange partial differential equations (PDEs) into image processing which was mostly treated in the discrete matrix setting before [5]. In improving this model, Caselles et al. [14] gave a geodesic active contour model to overcome the weakness of the above model and in particular allow topology changes of the evolving curves through embedding a level set function. Mumford and Shah [34] proposed the most celebrated variation model for segmentation of images with piecewise smooth intensity. The model cannot be implemented directly and easily. Ambrosio and Tortorelli [3] approximated the Mumford-Shah model by using simplified measures of an edge length term through introducing a smoothed region for the edges (jumps). Shen [40] considered the special case of the Ambrosio and Tortorelli model for piecewise constant images. Also for images with piecewise constant intensity, Chan and Vese [18] implemented the Mumford and Shah model for two phases using a level set representation and for multiphases Vese and Chan [17, 44] similarly found a way to implement the Mumford-Shah model. Another useful class of multiphase global segmentation models is the piecewise constant level method of Tai et al. [43] which only needs a single level set function to represent multiple phases. While gradient descent methods have been most widely used, fast and reliable algorithms for some of these models have been proposed in [6, 7, 24, 43].

The above variational models aim to segment a given image to find *all* meaningful objects within it. However in some applications e.g. medical diagnosis, surgery simulation, object tracking etc., it is absolutely necessary to locate a particular object among all objects in an image. For instance, a specialist doctor in diagnosis of a disease progression of a particular organ is only interested in the interested organ, not even adjacent organs while, understandably, when monitoring a particular suspect in a large crowd, one is only interested in precisely locating the intended suspect, not any other irrelevant people. Of course, one may start evolving an active contour from within or near the desired object and hope to locate its precise boundary. This works well for some problems. However unless neighbouring objects are far apart, the above global minimization models cannot reliably locate a single object.

Recently Gout et al. [22] and Badshah and Chen [8] proposed different selective segmentation models to tackle this feature selection problem. Both models are effective for segmenting a class of images. The former is a geodesic active contour model of parabolic PDEs; since it is an edge based model, its main weakness (as shared by all edge based models) is a lack of robustness in dealing with image noise. The latter model combined the edge detection ideas of the former with global domain based energy minimization idea of [18], resulting in improved robustness in dealing with image noise. However for some problems, both models can fail or cannot isolate a single and intended object; often adjacent objects as well as the intended object are picked up. In fact, if adjacent objects have a similar image intensity value C_1 to the intended object, the Badshah and Chen [8] model will converge to all such objects having similar image intensity of value C_1 i.e. the model fails to achieve the desired object selection; stopping the iteration early is one way of getting good

approximations. In some cases, one may observe the unfortunate scenario where an evolving curve passes through the boundary of the desired object and moves away from it instead of stopping. This motivates us to think about a way of using local intensity information to inform the model to stop at intended object boundaries.

In the literature, the concept of local geometric information has been used several times before [45, 37, 26, 27, 33, 35, 39]. The first idea is to use the numerical methodology by [30, 1, 2, 39] known as fast marching methods, which were later extended in [23], through evolving boundary contours in a neighbourhood of the underlying zero level set curves instead of solving for the level set function in the entire image domain. The second idea is to build narrow band approximations into the variational formulation [27, 33]. Our preliminary results from using the second idea by adopting the Lankton et al. [26] and Mille [33] methods in a narrow band variant of the Badshah and Chen [8] model suggest that the improvement is visible but it can still not deal with some examples for selective segmentation. The major problem with a fixed narrow band around the evolving contour is that the choice of band width is problem dependent; if the width is too large, the active contour is likely to pass through object boundary and detect other neighboring objects and if it is small, the active contour may not always evolve towards the desired image boundary.

In this paper, we propose an adaptively varying narrow band algorithm to segment a large class of image problems, particularly problems that cannot be segmented by the previous methods and the fixed narrow band method.

The rest of this paper is organized as follows. In Section 2, we briefly review the Chan-Vese segmentation model [18] and the image selective segmentation model by Badshah and Chen [8]. In Section 3, we first present a fixed γ -band method (F-M) based on local image features and a narrow band region, aiming to capture only local image intensity surrounding zero level and selectively extract one marked object from a given image. Then we give our variable γ -band method (V-M) and analyze the local function $b(\phi, \gamma)$ to highlight the performances of our proposed model. The gradient descent method [18, 16, 17, 42] is employed to solve the our minimization models. In Section 4, we show some numerical results using our new model for both synthetic and medical images in addition to comparing with the Badshah-Chen method [8], a global method and the Lankton-method [26]. We conclude this paper in Section 5.

To proceed, let the image domain $\Omega \subset \mathbb{R}^2$ be open and bounded, $f = f(x)$ be the given image and $\phi : \Omega \rightarrow \mathbb{R}$ be a Lipschitz continuous level set function in Ω . Then $\Gamma = \{x \in \Omega : \phi(x) = 0\}$ is the zero level set (curve), that will divide Ω into two segmented domains:

$$\Omega_{in} = \{x \in \Omega : \phi(x) < 0\}, \quad \Omega_{out} = \{x \in \Omega : \phi(x) > 0\}$$

with $\Omega = \Omega_{in} \cup \Gamma \cup \Omega_{out}$. Let $\nabla \phi(x_1, x_2) = (\phi_{x_1}, \phi_{x_2})$ be the gradient of the level set function $\phi(x)$, where $\phi_{x_j} = \frac{\partial \phi}{\partial x_j}$, $j = 1, 2$. Let $\mathcal{A} = \{\hat{x}_i : i = 1 \dots n_p\}$ is a marker set which is given on or near the boundary of a detected object in a given image $f(x)$ which can be used to define an initial contour and to guide its evolution towards Γ .

2. Review of two existing models. In this section, we mainly review the Chan-Vese model [18] as an example of a global segmentation model and the Badshah and Chen image selective segmentation model [8] of combining geometrical constraints with the piecewise constant intensity fitting conditions. The latter model finds

the desired interface Γ by minimizing of an energy functional under several given markers.

Denote by $H(z)$ the Heaviside function and by $\delta(z) = H'(z)$ the Delta function. Then the length of Γ can be computed by $\int_{\Omega} g(x)|\nabla H(\phi(x))|dx$. In implementations, both $H(z)$ and $\delta(z)$ shall be regularized as follows [18, 19, 45, 35]:

$$(1) \quad H_{\epsilon}(z) = \begin{cases} 1, & z > \epsilon; \\ (\frac{z}{2\epsilon} + \frac{1}{2\pi} \sin \frac{\pi z}{\epsilon} + 1), & |z| \leq \epsilon; \\ 0, & z < -\epsilon, \end{cases} \quad \delta_{\epsilon}(z) = \begin{cases} \frac{1}{2\epsilon}(1 + \cos \frac{\pi z}{\epsilon}), & |z| \leq \epsilon; \\ 0, & |z| > \epsilon, \end{cases}$$

where $\delta_{\epsilon}(z) = H'_{\epsilon}(z)$, or alternatively

$$H_{\epsilon}(z) = \frac{1}{2}(1 + \frac{2}{\pi} \arctan(\frac{z}{\epsilon})), \quad H_{\epsilon}(z) = \begin{cases} 1, & z > \epsilon; \\ -\frac{z^3}{4\epsilon^3} + \frac{3z}{4\epsilon} + \frac{1}{2}, & |z| \leq \epsilon; \\ 0, & z < -\epsilon. \end{cases}$$

Finally denote by $\vec{n} = \frac{\nabla\phi}{|\nabla\phi|}$ the normal direction on level lines of ϕ and the mean curvature by $\kappa = \nabla \cdot \frac{\nabla\phi}{|\nabla\phi|}$; refer to [35].

2.1. The Chan-Vese model. The Chan and Vese model [18] considers the simple case where the image $f(x)$ can be approximated by two regions of piecewise constant image intensity, separated by the boundary Γ . Denote these (unknown) intensity values by C_1 and C_2 . Assume that the region of interest is represented by C_1 inside Γ whereas, outside Γ , the intensity of $f(x)$ is approximately C_2 .

The Chan-Vese model minimises the following energy functional

$$(2) \quad E(\Gamma, C_1, C_2) = \int_{\Gamma} ds + \left\{ \int_{\Omega_{in}} (f(x) - C_1)^2 dx + \int_{\Omega_{out}} (f(x) - C_2)^2 dx \right\}$$

where C_1 and C_2 are two constants that respectively approximate the image intensity in Ω_{in} and Ω_{out} . This is a reduced Mumford-Shah functional introduced in [34] for a general piecewise smooth image $f(x)$ which is not amenable to direct implementation; approximations to the Mumford-Shah functional can lead to amenable implementations [3, 19]. With a level set formulation, the above energy minimization problem can be written as

$$(3) \quad E_{\epsilon}(\phi, C_1, C_2) = \int_{\Omega} \delta_{\epsilon}(\phi(x))|\nabla\phi(x)|dx + \left\{ \int_{\Omega} [1 - H_{\epsilon}(\phi(x))](f(x) - C_1)^2 dx + \int_{\Omega} H_{\epsilon}(\phi(x))(f(x) - C_2)^2 dx \right\}.$$

Firstly keeping the level set function $\phi(x)$ fixed and minimizing the functional $E_{\epsilon}(\phi, C_1, C_2)$ with respect to C_1 and C_2 , one derives

$$(4) \quad C_1 = \frac{\int_{\Omega} [1 - H_{\epsilon}(\phi(x))]f(x)dx}{\int_{\Omega} [1 - H_{\epsilon}(\phi(x))]dx}, \quad C_2 = \frac{\int_{\Omega} H_{\epsilon}(\phi(x))f(x)dx}{\int_{\Omega} H_{\epsilon}(\phi(x))dx}.$$

Secondly fixing constants C_1 and C_2 in $E_\epsilon(\phi, C_1, C_2)$, by first variations with respect to $\phi(x)$, then we derive the following level set evolution equation:

$$(5) \quad \begin{aligned} \frac{\partial \phi}{\partial t} &= \delta_\epsilon(\phi) \nabla \cdot \left(\frac{\nabla \phi}{|\nabla \phi|} \right) + \delta_\epsilon(\phi) \left\{ (f(x) - C_1)^2 - (f(x) - C_2)^2 \right\}, \\ \frac{\delta_\epsilon(\phi)}{|\nabla \phi|} \frac{\partial \phi}{\partial \vec{n}} &= 0 \quad \text{on} \quad \partial \Omega. \end{aligned}$$

The above model offers a very powerful, flexible method that can successfully segment many types of images, including some that would be difficult or impossible to segment with edge-based methods. Of course, there exist many other methods for global segmentation; see [19, 29, 43] and the references therein. In addition, Chan, Esedoglu and Nikolova [15] proposed a convex approach to improve the Chan-Vese model for solving noise removal and image segmentation problems; Brown, Chan and Bresson [10] developed a multi-phase piecewise constant image segmentation model based on convex approach, more details also refer to [9, 21, 11]. Such models overcame sensitivity of Chan-Vese model employing the level set formulation to the initialization and the selection of parameters, though they still are global segmentation models (extract all such objects having similar image intensity, not one satisfying the expected selection requirement). Hence, whenever the functionality of selectivity is needed, global segmentation methods are not suitable. For example in Fig. 10, we might like to segment the right kidney only whilst the above methods will give the kidney along with other organs. With any subsequent manual selection, this defeats the objective of automatic segmentation.

2.2. The Badshah-Chen model. To only detect the boundary of a single object among all homogeneity intensity objects, improving on the edge-based model of Gout et al. [22], Badshah and Chen [8] proposed an image selective segmentation energy functional combining edge detection under geometrical constraints with intensity fitting terms similar to Chan-Vese [18] as follows:

(6)

$$\begin{aligned} E(\Gamma, C_1, C_2) &= \alpha E_{\text{edge}}(\Gamma) + E_{\text{fitting}}(\Gamma, C_1, C_2) \\ &= \alpha \int_{\Gamma} d(x)g(x)ds + \left\{ \lambda_1 \int_{\Omega_{in}} |f(x) - C_1|^2 dx + \lambda_2 \int_{\Omega_{out}} |f(x) - C_2|^2 dx \right\}. \end{aligned}$$

This model delivers the objective of selectivity and inherits the advantages of the Chan-Vese model: (i) it can detect contours of the image with low variations of intensity gradients; (ii) it also can segment a noisy image without smoothing the image. Using a level set formulation, they derived first the Euler-Lagrange equation from minimizing the energy and then the following evolution equation (6):

$$(7) \quad \frac{\partial \phi}{\partial t} = \delta_\epsilon(\phi) \left(\alpha \nabla \cdot \left(d(x)g(x) \frac{\nabla \phi}{|\nabla \phi|} \right) + \lambda_1 (f(x) - C_1)^2 - \lambda_2 (f(x) - C_2)^2 \right)$$

where $d(x)$ is a marker distance function, which is close to zero when towards the given markers and to one elsewhere, and $g(x)$ is an edge detector function which is constructed to take small values (towards 0) near image edges and large values (towards 1) in flat regions.

As with methods of geodesic active contours, the idea behind $g(x)$ is that the large gradient $|\nabla f(x)|$ of image $f(x)$ indicates an edge so in most active contours

models [14, 8, 19, 22, 25] a decreasing function g of the gradient $|\nabla f(x)|$ is chosen as an edge detector. A typical example in image segmentation is the following

$$g(x) = \frac{1}{1 + a|\nabla f(x)|^2}$$

with $a > 0$, and there also exist other variants [19] e.g. $g(x) = \exp(-b|\nabla f(x)|^s)$, $b > 0, s > 0$ or $g(x) = -|\nabla f(x)|^2$ – a negative function. To deal with noise, $\nabla f(x)$ shall be replaced by its smoothing image ∇f_σ . We remark that a related but less commonly used nonlinear choice is to take $g(u(x)) = e^{iv}/(1 + (Im(u)/kv)^2)$, with $v \geq 0, k > 0$, in a complex formulation [20, 4]. In [22, 8], the following distance function is used:

$$(8) \quad d(x) = d_1(x) = \prod_{i=1}^{n_p} \left(1 - \exp\left(-\frac{|x - \hat{x}_i|^2}{2\sigma^2}\right)\right)$$

where normally $\sigma = 4$ or $\sigma = 3$. Another distance function is presented in [22] as follows:

$$(9) \quad d(x) = d_2(x) = \frac{\min_{\hat{x}_i \in \mathcal{A}} |x - \hat{x}_i|}{\max_{\hat{x}_i \in \mathcal{A}} \max_{\bar{x} \in \Omega} |\bar{x} - \hat{x}_i|} = \frac{1}{M} \min_{\hat{x}_i \in \mathcal{A}} |x - \hat{x}_i|.$$

Clearly with the above choices for equation (7), the contour Γ is encouraged to evolve into the neighborhood of markers by optimizing $d(x)$, while it is to stop on edges (i.e. high values of the gradient) of the desired object by optimizing $g(x)$. This is true if the last 2 terms of (7) are not dominant.

At initial iterations, the coefficient $g(x)d(x)$ is not yet small. To encourage faster evolution, a ‘balloon’ force term $\beta d(x)g(x)|\nabla \phi(x)|$ is added [8] to the equation (7) to attract the contours to the correct boundaries where $g(x)d(x) \approx 0$ as used by [14, 22] previously.

However the Badshah-Chen model [8] is only a practical model and not a theoretically robust model, because asymptotically its solution is dominated by global image intensity fitting terms and tends to that of global segmentation (i.e. capturing all objects having similar image intensity). Since in some applications it is absolutely necessary to segment a particular object among all similar intensity objects, there is an urgent need for local and selective models. This is rather like the case of an inverse scale-space method for image denoising [12], starting from a clean and flat image and converging to the noisy image. As shown in Fig.1 for model [8], the contour is already evolved into Γ (which is the intended extraction) at (a) but the method has not converged, while (b-c) are already too late to stop. Here, the test image in Fig.1 is of size for 512×512 with $f(x) : \Omega \rightarrow [0 \ 255]$, $\alpha = 0.1 \times 255^2$ and $\lambda_1 = \lambda_2 = 1$. Fig.1(b) is the result after 200 iterations (passing through the desired solution of a concave box satisfying the expected selection requirement). The final result stops in incorrect contours of Figure 1(c) after 642 iterations. The Badshah-Chen model fails to segment selectively this concave box. Clearly, it is crucial to know when to terminate iterations, before converging to the wrong solution. This motivates us in this paper to use different fitting terms and to stop automatically.

3. An improved model based on local features. The primary aim of this section is to present our new selective segmentation model to overcome the drawbacks of [8]. To introduce it, our initial model is based on local intensity information [33]

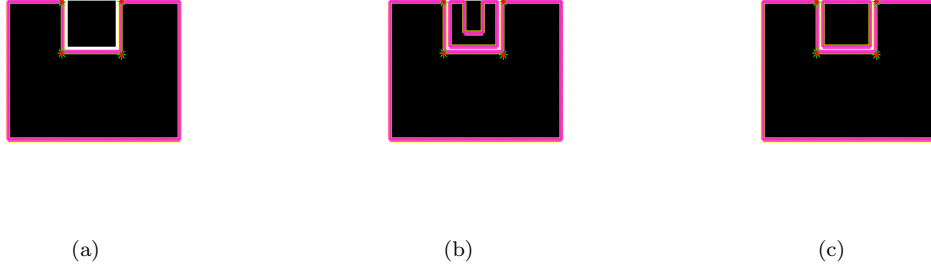


FIG. 1. Evolving sequences of the Badshah-Chen method passing through the desirable solution of (a).

of the segmented image and geometrical constraints as in [8], so only pixels in a neighborhood (i.e. a fixed narrow band region) of zero level curve are used in data fitting; we hope other homogenous objects do not attract the contour. It turns out that this initial model does improve on [8] but it is not robust enough with respect to the fixed band width. We further propose a robust variable band model which selects the band width adaptively as the curve evolves.

Below we shall give first our fixed band model and then our recommended variable band model.

3.1. A Fixed- γ Method based on local features. We first generalize the Badshah-Chen model [8] to a local constrained minimization segmentation model (denoted by F-M) using narrow band fitting terms

$$(10) \quad \min_{\Gamma, C_1, C_2} \left\{ E(\Gamma, C_1, C_2) = \alpha E_G(\Gamma) + E_F(\Gamma, C_1, C_2) \right\}$$

where $E_G(\Gamma) = \int_{\Gamma} G(x) ds$ and $G(x) = g(x)d(x)$ as in Badshah and Chen [8], and

$$(11) \quad E_F(\Gamma, C_1, C_2) = \left\{ \lambda_1 \int_{\Omega_{in}(\Gamma)} (f(x) - C_1)^2 dx + \lambda_2 \int_{\Omega_{out}(\Gamma)} (f(x) - C_2)^2 dx \right\},$$

with $\Omega_{in}(\Gamma)$ and $\Omega_{out}(\Gamma)$ denoting the γ -band inside and outside region from Γ respectively as in [33]. Since we assume that ϕ is negative inside the desired region and positive outside it, then the local fitting energy function

$$(12) \quad b(\phi(x), \gamma) = H(\phi(x) + \gamma)(1 - H(\phi(x) - \gamma))$$

characterizes the domain $\Omega_{\gamma} = \Omega_{in}(\Gamma) \cup \Gamma \cup \Omega_{out}(\Gamma)$ which is a narrow band region surrounding the local boundary Γ ; inside Ω_{γ} , $b = 1$ and elsewhere $b = 0$. Other local energies [26, 27] may also be introduced into this model.

From properties of the Heaviside function $H(\phi)$, i.e. $(1 - H(\phi))b(\phi(x), \gamma) = 1$ in $\Omega_{in}(\Gamma)$ and $H(\phi)b(\phi(x), \gamma) = 1$ in $\Omega_{out}(\Gamma)$, the above optimization problem (10) can be rewritten as:

$$\min_{\phi, C_1, C_2} \alpha \int_{\Omega} G(x) |\nabla H(\phi)| dx + \left\{ \lambda_1 \int_{\Omega} (1 - H(\phi)) b(\phi(x), \gamma) (f(x) - C_1)^2 dx \right.$$

$$(13) \quad + \lambda_2 \int_{\Omega} H(\phi)b(\phi(x), \gamma)(f(x) - C_2)^2 dx \Big\}$$

Further when the level set function ϕ is fixed, the local mean intensity values C_1 , C_2 respectively inside and outside regions of a zero level set curve are given by:

$$(14) \quad C_1 = \frac{\int_{\Omega}(1 - H(\phi))b(\phi(x), \gamma)f(x)dx}{\int_{\Omega}(1 - H(\phi))b(\phi(x), \gamma)dx}, \quad C_2 = \frac{\int_{\Omega}H(\phi)b(\phi(x), \gamma)f(x)dx}{\int_{\Omega}H(\phi)b(\phi(x), \gamma)dx}.$$

When C_1, C_2 are fixed, we calculate the *Gâteaux* derivatives of the energy functional in (13) and deduce the following Euler-Lagrange equation for ϕ :

$$(15) \quad \begin{aligned} & -\alpha\delta_{\epsilon}\nabla \cdot \left(G(x) \frac{\nabla\phi}{|\nabla\phi|} \right) - \lambda_1 \left[\delta_{\epsilon}(\phi)b(\phi, \gamma) - (1 - H_{\epsilon}(\phi)) \frac{\partial b(\phi, \gamma)}{\partial\phi} \right] (f - C_1)^2 \\ & + \lambda_2 \left[\delta_{\epsilon}(\phi)b(\phi, \gamma) + \frac{\partial b(\phi, \gamma)}{\partial\phi} H_{\epsilon}(\phi) \right] (f - C_2)^2 = 0; \\ & G(x) \frac{\delta_{\epsilon}(\phi)}{|\nabla\phi|} \frac{\partial\phi}{\partial n} \Big|_{\partial\Omega} = 0, \end{aligned}$$

where H_{ϵ} is a regularised Heaviside function by (1). The above PDE may be solved by a gradient descent method as used by [19, 35].

For practical applications our F-M is stopped if the maximum number of gradient descent iterations is reached (usually $it = 3000$), or the relative error in two consecutive iterative steps is smaller than a small number $\eta_0 > 0$ (typically $\eta_0 = 10^{-11}$ for a convergence test and only $\eta_0 = 10^{-6}$ for a practical segmentation), or the number of entire inner pixels of zero level is smaller than 10. Here let *ELFM_{local}* denote the time marching evolving process solving the Euler-Lagrange equation (15), where the previous step ϕ^n and band width $\bar{\gamma}$ are fixed. A pseudo-code implementation of our F-M is then summarized in the following algorithm:

Algorithm 1 (A Fixed- γ Method based on local features).

- step 1. Input markers set: $\mathcal{A} = \{\bar{x}^{\ell} = (x_1^{\ell}, \dots, x_m^{\ell})^T : \ell = 1, \dots, \bar{\ell}\}$, $m = 2$ for 2D problem and $m = 3$ for 3D problem. Set the localizing parameter: inner $\bar{\gamma}$ and the initial level set function ϕ^0 . Set $n = 0$ and $it = 2$.*
- step 2. Re-initialize the level set function ϕ^n .*
- step 3. Solve the evolving equation (15):*
- $\phi^{n+1} = ELFM_{local}(\phi^n, \bar{\gamma}, it)$;
- step 4. Check for convergence using the above criteria.*
- If not satisfied; set $n = n + 1$ and go to step 3.;
- Else return solution $\phi^ = \phi^{n+1}$;*

We remark that this model is based on geodesic active contours and local intensity fitting conditions in which an edge detector attracts the curve to the boundary of an object once an active contour is close to the boundary. Since local region terms are more likely to capture the mean intensity of the inside and outside regions immediately around zero level curves than global fitting terms, such a model can segment selectively an object with weak edges (i.e. low intensity contrast near edges) than the previous model [8], provided that the initial contour is suitable and

the user supplied band width γ is appropriate. As we see, the latter assumptions turn out to be the main weak points of the F-M model – essentially the localizing parameter γ is sensitive and image dependent in order for the model to achieve selectivity all the time.

Specifically, since the localizing parameter γ drives the local function $b(\phi, \gamma)$ in energy functional $E(\phi, C_1, C_2)$ in a dominant way, a small γ helps $b(\phi, \gamma)$ to capture less image features and the contour may stop the steady state without reaching the intended object boundary or shrink to a point. Conversely if γ is too large, the active contour is likely to detect other objects which would also fail the selectivity functionality of the model.

3.2. A Variable- γ method based on local features. The central question is how to select γ automatically because it is in general unknown *a priori*. But we know that intensity variations within inner and outer narrow regions are approximately zero when the zero level curve stops on the object boundary. This observation can be explored by varying the band widths in order to automatically select the band width that helps reducing such intensity variations. This locally optimal band width leads to our variable- γ method. Therefore the basic idea for finding the optimal γ automatically is to select from the extremal points of two functions (defined shortly): a mean intensity variation function and a local mean intensity variation function with respect to the localizing parameter γ surrounding the zero level curve.

In our proposed method below, we shall treat $\Omega_{in}(\Gamma)$ and $\Omega_{out}(\Gamma)$ separately and hence there is no need to use the same γ parameter. To this end, we shall redefine them using different γ 's. In particular, let $\Omega_{in}(\Gamma)$ denote the γ_{in} -band inside region from Γ and $\Omega_{out}(\Gamma)$ the γ_{out} -band outside region from Γ . Then we redefine the local fitting energy function as

$$(16) \quad b(\phi(x), \gamma_{in}, \gamma_{out}) = H(\phi(x) + \gamma_{in})(1 - H(\phi(x) - \gamma_{out}))$$

which characterizes the narrow band domain $\Omega_{\gamma_{in}, \gamma_{out}} = \Omega_{in}(\Gamma) \cup \Gamma \cup \Omega_{out}(\Gamma)$ which is a narrow band region surrounding the local boundary Γ . As before inside $\Omega_{\gamma_{in}, \gamma_{out}}$, $b = 1$ and elsewhere $b = 0$. Even with two parameters $\gamma_{in}, \gamma_{out}$, as long as they are fixed, the local model will be similar to F-M. That is, we solve

$$(17) \quad \min_{\phi, C_1, C_2} \alpha \int_{\Omega} G(x) |\nabla H(\phi)| dx + \left\{ \lambda_1 \int_{\Omega} (1 - H(\phi)) b(f(x) - C_1)^2 dx + \lambda_2 \int_{\Omega} H(\phi) b(f(x) - C_2)^2 dx \right\}$$

instead of (13) and the main level set equation

$$(18) \quad -\alpha \delta_{\epsilon} \nabla \cdot \left(G(x) \frac{\nabla \phi}{|\nabla \phi|} \right) - \lambda_1 \left[\delta_{\epsilon}(\phi) b - (1 - H_{\epsilon}(\phi)) \frac{\partial b}{\partial \phi} \right] (f - C_1)^2 + \lambda_2 \left[\delta_{\epsilon}(\phi) b + \frac{\partial b}{\partial \phi} H_{\epsilon}(\phi) \right] (f - C_2)^2 = 0,$$

instead of (15), where $b = b(\phi(x), \gamma_{in}, \gamma_{out})$. In each optimization step, we first choose optimized $\gamma_{in}, \gamma_{out}$ and then update C_1, C_2, ϕ .

However, our idea below is to select $\gamma_{in}, \gamma_{out}$ in an automatic way. The selection is based on changes of the fitting terms as a function of such band parameters. Minimizing such a function locally provides the optimized band widths. Once this is done, our resulting model will be a variable γ -model (to be denoted by V-M).

To proceed, we first discuss γ_{in} and the inside band region Ω_{in} . Note $[1 - H(\phi)]b(\phi, \gamma_{in}, \gamma_{out}) = [1 - H(\phi)]H(\phi + \gamma_{in})$ which is 1 inside Ω_{in} and 0 elsewhere. In Ω_{in} , define its mean intensity variation function $MIV_{in}(\gamma_{in})$ for a given level set function ϕ as the derivation from its mean intensity $MI_{in}(\gamma_{in})$ by

$$(19) \quad \begin{aligned} MIV_{in}(\gamma_{in}) &= \left\{ \frac{\int_{\Omega} [1 - H(\phi)]H(\phi + \gamma_{in})[f(x) - MI_{in}(\gamma_{in})]^2 dx}{\int_{\Omega} [1 - H(\phi)]H(\phi + \gamma_{in}) dx} \right\}^{\frac{1}{2}}, \\ MI_{in}(\gamma_{in}) &= \frac{I_{in}(\gamma_{in})}{\int_{\Omega} [1 - H(\phi)]H(\phi + \gamma_{in}) dx}, \\ I_{in}(\gamma_{in}) &= \int_{\Omega} [1 - H(\phi)]H(\phi + \gamma_{in})f(x) dx. \end{aligned}$$

An extremal point set of $MIV_{in}(\gamma)$ in $[\gamma_{min}-1, \gamma_{max}]$ can be defined by:

$$\Theta_{in} = \left\{ \gamma : \left(\arg \max_{\gamma_{min}-1 < \gamma \leq \gamma_{max}} MIV_{in}(\gamma) \right) \cup \left(\arg \min_{\gamma_{min}-1 < \gamma \leq \gamma_{max}} MIV_{in}(\gamma) \right) \right\}$$

where we assume $\gamma_{min}, \gamma_{max}$ are two given bandwidths with $\gamma_{max} > \gamma_{min} > 1$ and in the discrete setting $\gamma_{min} \geq 2$. See Fig.3(b) for one illustrating example of these definitions.

If $\min_{\gamma} \Theta_{in} < \gamma_{max}$, then it is a suitable candidate for γ_{in} . If not, i.e. $\min_{\gamma} \Theta_{in} = \gamma_{max}$, we have to use an extra test to see if $\gamma_{in} = \gamma_{max}$ is appropriate as unnecessarily large γ_{in} might help the evolving curve to capture nearby objects. Note that for a fixed band gap $\delta\gamma > 0$, the quantity $[1 - H(\phi)][H(\phi + \gamma + \delta\gamma) - H(\phi + \gamma)]$ defines the narrow strip of width $\delta\gamma$ near the narrow band γ . This further test is based on the local mean intensity variation function $LMIV_{in}(\gamma)$ within this band gap:

$$(20) \quad \begin{aligned} LMI_{in}(\gamma) &= \frac{I_{in}(\gamma + \delta\gamma) - I_{in}(\gamma)}{\int_{\Omega} [1 - H(\phi)][H(\phi + \gamma + \delta\gamma) - H(\phi + \gamma)] dx}; \\ LMIV_{in}(\gamma) &= \left\{ \frac{K}{\int_{\Omega} [1 - H(\phi)][H(\phi + \gamma + \delta\gamma) - H(\phi + \gamma)] dx} \right\}^{\frac{1}{2}}, \end{aligned}$$

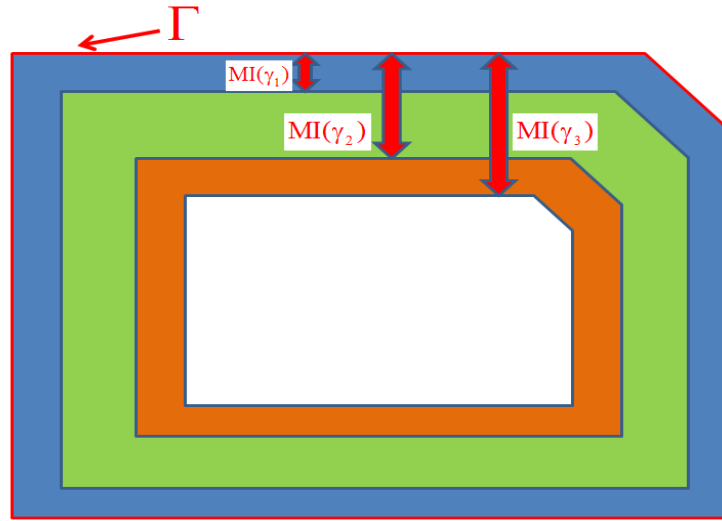
where $K = \int_{\Omega} [1 - H(\phi)][H(\phi + \gamma + \delta\gamma) - H(\phi + \gamma)][f(x) - LMI_{in}(\gamma, \delta\gamma)]^2 dx$. Define an extremal point set of $LMIV_{in}(\gamma)$ in $[\gamma_{min}-1, \gamma_{max}]$ by:

$$\Xi_{in} = \left\{ \gamma : \left(\arg \max_{\gamma_{min}-1 < \gamma \leq \gamma_{max}} LMIV_{in}(\gamma) \right) \cup \left(\arg \min_{\gamma_{min}-1 < \gamma \leq \gamma_{max}} LMIV_{in}(\gamma) \right) \right\}.$$

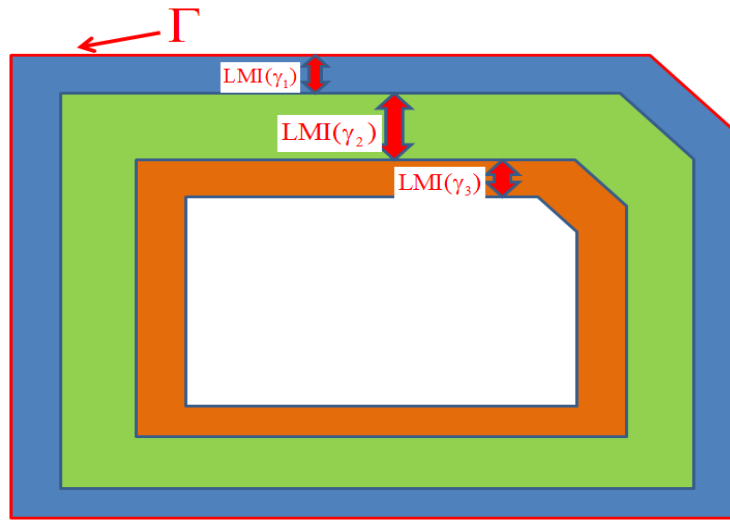
Then in this case, $\min_{\gamma} \Xi_{in}$ is a suitable choice for γ_{in} . Fig.2 illustrates the setup of the above two definitions for a simple and evolving boundary Γ . Therefore the local parameter γ_{in} describing the local inside domain Ω_{in} is automatically selected by

$$\check{\gamma}_{in} = \begin{cases} \min_{\gamma} \Theta_{in}, & \text{if } \min_{\gamma} \Theta_{in} < \gamma_{max}; \\ \min_{\gamma} \Xi_{in}, & \text{otherwise.} \end{cases}$$

Similarly to the inner γ_{in} -choice, the procedure for selecting γ_{out} only requires minor modifications since the main change is to replace the local characteristic function $[1 - H(\phi)]b(\phi, \gamma_{in}, \gamma_{out}) = [1 - H(\phi)]H(\phi + \gamma_{in})$ for domain Ω_{in} by $H(\phi)b(\phi, \gamma_{in}, \gamma_{out})$



(a)



(b)

FIG. 2. Illustration of domains for mean intensity calculations (Top: MI and Bottom: LMI).

$= H(\phi)[1 - H(\phi - \gamma_{out})]$ for the local domain Ω_{out} . The modified formulae are

$$\begin{aligned}
 I_{out}(\gamma) &= \int_{\Omega} H(\phi)[1 - H(\phi - \gamma)]f(x)dx; \\
 MI_{out}(\gamma) &= \frac{I_{out}(\gamma)}{\int_{\Omega} H(\phi)[1 - H(\phi - \gamma)]dx}; \\
 MIV_{out}(\gamma) &= \left\{ \frac{\int_{\Omega} H(\phi)[1 - H(\phi - \gamma)](f(x) - MI_{out}(\gamma))^2 dx}{\int_{\Omega} H(\phi)[1 - H(\phi - \gamma)]dx} \right\}^{\frac{1}{2}};
 \end{aligned}
 \tag{21}$$

$$LMI_{out}(\gamma) = \frac{I_{out}(\gamma + \delta\gamma) - I_{out}(\gamma)}{\int_{\Omega} H(\phi)[H(\phi - \gamma) - H(\phi - \gamma - \delta\gamma)]dx};$$

$$LMIV_{out}(\gamma) = \left\{ \frac{K_1}{\int_{\Omega} H(\phi)[H(\phi - \gamma) - H(\phi - \gamma - \delta\gamma)]dx} \right\}^{\frac{1}{2}},$$

where $K_1 = \int_{\Omega} H(\phi)[H(\phi - \gamma) - H(\phi - \gamma - \delta\gamma)][f(x) - LMI_{out}(\gamma, \delta\gamma)]^2 dx$, and Θ_{out} , Ξ_{out} are similarly defined. Hence

$$\gamma_{out} = \begin{cases} \min_{\gamma} \Theta_{out}, & \text{if } \min_{\gamma} \Theta_{out} < \gamma_{max}; \\ \min_{\gamma} \Xi_{out}, & \text{otherwise.} \end{cases}$$

In numerical implementations, in a discrete setting, we naturally take positive integers for $\gamma_{in}, \gamma_{out}$ and set $\delta\gamma = 1$. Then Θ_{in} and Ξ_{in} can be simplified to the following $\bar{\Theta}_{in}$ and $\bar{\Xi}_{in}$ respectively:

$$\begin{aligned} \bar{\Theta}_{in} = & \{ \gamma_{max} \} \cup \{ \gamma \in N : \gamma_{min} \leq \gamma \leq \gamma_{max} \text{ such that} \\ & MIV(\gamma) \leq MIV(\gamma - 1) \text{ and } MIV(\gamma) < MIV(\gamma + 1) \} \\ & \cup \{ \gamma \in N : \gamma_{min} \leq \gamma \leq \gamma_{max} \text{ such that} \\ & MIV(\gamma) \geq MIV(\gamma - 1) \text{ and } MIV(\gamma) > MIV(\gamma + 1) \}; \\ \bar{\Xi}_{in} = & \{ \gamma_{max} \} \cup \{ \gamma \in N : \gamma_{min} \leq \gamma \leq \gamma_{max} \text{ such that} \\ & LMIV(\gamma) \leq LMIV(\gamma - 1) \text{ and } LMIV(\gamma) < LMIV(\gamma + 1) \} \\ & \cup \{ \gamma \in N : \gamma_{min} \leq \gamma \leq \gamma_{max} \text{ such that} \\ & LMIV(\gamma) \geq LMIV(\gamma - 1) \text{ and } LMIV(\gamma) > LMIV(\gamma + 1) \}. \end{aligned}$$

We also remark that small oscillations may be associated with the computed quantities $MIV_{\iota}(\gamma)$ and $LMIV_{\iota}(\gamma)$ (with $\iota = 'in'/'out'$) if image noise is present. To alleviate the effect of image noise or false boundaries, then all we need to do is to replace absolute inequality tests by relative inequality ones, e.g., the comparison of $MIV_{\iota}(\gamma_i), MIV_{\iota}(\gamma_{i+1})$ is replaced by $|MIV_{\iota}(\gamma_i) - MIV_{\iota}(\gamma_{i+1})| < \eta_3 |MIV_{\iota}(\gamma_i) + MIV_{\iota}(\gamma_{i+1})|$ for some $0 < \eta_3 < 1$ — if true, the difference is small and γ_i is not considered as an extremal point.

Now the overall procedure of finding an optimal γ_{ι} is summarized below in Algorithm 2. Using Algorithm 2, we would obtain two independent and optimized parameters $\check{\gamma}_{in}$ and $\check{\gamma}_{out}$. We hope to refine them, if they are quite different, in the case of both small gradient variations and small intensity variations in Ω_{in} as well as Ω_{out} ; the idea is to take large values in this case. Define the mean gradient variation in Ω_{in} and Ω_{out} respectively by

$$(22) \quad \begin{aligned} MGI_{in}(\check{\gamma}_{in}) &= \frac{\int_{\Omega} [1 - H(\phi)] H(\phi + \check{\gamma}_{in}) |\nabla f(x)| dx}{\int_{\Omega} [1 - H(\phi)] H(\phi + \check{\gamma}_{in}) dx}; \\ MGI_{out}(\check{\gamma}_{out}) &= \frac{\int_{\Omega} H(\phi) [1 - H(\phi - \check{\gamma}_{out})] |\nabla f(x)| dx}{\int_{\Omega} H(\phi) [1 - H(\phi - \check{\gamma}_{out})] dx}. \end{aligned}$$

Then the special case that we are concerned with is when

$$\frac{|MI_{in}(\check{\gamma}_{in}) - MI_{out}(\check{\gamma}_{out})|}{|MI_{in}(\check{\gamma}_{in}) + MI_{out}(\check{\gamma}_{out})|} < \frac{\eta_1}{2} \quad \text{and} \quad \frac{|MGI_{in}(\check{\gamma}_{in}) - MGI_{out}(\check{\gamma}_{out})|}{|MGI_{in}(\check{\gamma}_{in}) + MGI_{out}(\check{\gamma}_{out})|} < \frac{\eta_2}{2}$$

for some small η_1, η_2 such that $0 < \eta_1, \eta_2 < 1$. If so, unless $\check{\gamma}_{in} = \check{\gamma}_{out}$, we will set the smallest quantity to be γ_{max} .

Algorithm 2 (Inner or outer γ -choice).
 $\tilde{\gamma} = \text{Band_width}(\gamma_{min}, \gamma_{max}, \eta_3, \iota)$
 $\% \iota = 'in'$ — compute inner γ -choice;
 $\% \iota = 'out'$ — compute outer γ -choice.
Step 1. set $i=1$; $\gamma_0 = \gamma_{min} - 1$;
Step 2. find the first $\gamma_i > \gamma_{i-1}$ such that $\gamma_i \in \bar{\Theta}_\iota$;
Step 3. if $\gamma_i \neq \gamma_{max}$; find the first $\gamma_{i+1} > \gamma_i$ such that $\gamma_{i+1} \in \bar{\Theta}_\iota$;
 else set $\tilde{\gamma} = \gamma_i$ and go to step 5;
Step 4. if $|MIV_\iota(\gamma_i) - MIV_\iota(\gamma_{i+1})| < \eta_3|MIV_\iota(\gamma_i) + MIV_\iota(\gamma_{i+1})|$;
 - $i=i+2$, and go to step 2;
 else set $\tilde{\gamma} = \gamma_i$ and go to step 5;
Step 5. if $\tilde{\gamma} < \gamma_{max}$; return $\tilde{\gamma}$;
 else go to step 6;
Step 6. set $i=1$; $\gamma_0 = \gamma_{min} - 1$;
Step 7. find the first $\gamma_i > \gamma_{i-1}$ such that $\gamma_i \in \bar{\Xi}_\iota$;
Step 8. if $\gamma_i \neq \gamma_{max}$; find the first $\gamma_{i+1} > \gamma_i$ such that $\gamma_{i+1} \in \bar{\Xi}_\iota$;
 else set $\tilde{\gamma} = \gamma_i$ and return $\tilde{\gamma}$;
Step 9. if $|LMIV_\iota(\gamma_i) - LMIV_\iota(\gamma_{i+1})| < \eta_3|LMIV_\iota(\gamma_i) + LMIV_\iota(\gamma_{i+1})|$;
 - $i=i+2$, and go to step 7;
 else set $\tilde{\gamma} = \gamma_i$ and return $\tilde{\gamma}$.

So finally our implementation of the proposed γ -choice will be based on many quantities of inside and outside respectively: the mean variations $MIV(\gamma)$, the local mean variations $LMIV(\gamma)$, the mean values $MI(\tilde{\gamma})$ and the mean gradient variations $MGV(\tilde{\gamma})$ as summarized in the following Algorithm 3. Usually we fix

Algorithm 3 (A robust localizing parameter-choice algorithm (RLPCA)).
 $[\gamma_{in}, \gamma_{out}] = \text{RLPCA}(\gamma_{min}, \gamma_{max}, \eta_1, \eta_2, \eta_3)$
• Compute inner and outer band width via Algorithm 1:
- $\tilde{\gamma}_{in} = \text{Band_width}(\gamma_{min}, \gamma_{max}, \eta_3, 'in')$;
- $\tilde{\gamma}_{out} = \text{Band_width}(\gamma_{min}, \gamma_{max}, \eta_3, 'out')$.
• Compute $MI_{in}(\tilde{\gamma}_{in})$, $MI_{out}(\tilde{\gamma}_{out})$, $MGI_{in}(\tilde{\gamma}_{in})$ and $MGI_{out}(\tilde{\gamma}_{out})$; then
- If $\left| \frac{MI_{in}(\tilde{\gamma}_{in}) - MI_{out}(\tilde{\gamma}_{out})}{MI_{in}(\tilde{\gamma}_{in}) + MI_{out}(\tilde{\gamma}_{out})} \right| < \eta_1/2$ and $\left| \frac{MGI_{in}(\tilde{\gamma}_{in}) - MGI_{out}(\tilde{\gamma}_{out})}{MGI_{in}(\tilde{\gamma}_{in}) + MGI_{out}(\tilde{\gamma}_{out})} \right| < \eta_2/2$,
* if $\tilde{\gamma}_{in} < \tilde{\gamma}_{out}$
- $\gamma_{in} = \gamma_{max}$, $\gamma_{out} = \tilde{\gamma}_{out}$;
* elseif $\tilde{\gamma}_{in} > \tilde{\gamma}_{out}$
- $\gamma_{in} = \tilde{\gamma}_{in}$, $\gamma_{out} = \gamma_{max}$;
* else
- $\gamma_{in} = \tilde{\gamma}_{in}$, $\gamma_{out} = \tilde{\gamma}_{out}$.
* endif
- Else
- $\gamma_{in} = \tilde{\gamma}_{in}$, $\gamma_{out} = \tilde{\gamma}_{out}$.
- Endif

two γ constraints as $\gamma_{min} = 2$ and $\gamma_{max} = 30$, and the other parameters as follows: $\eta_1 = 0.1$, $\eta_2 = 0.2$ and $\eta_3 = 0.1$.

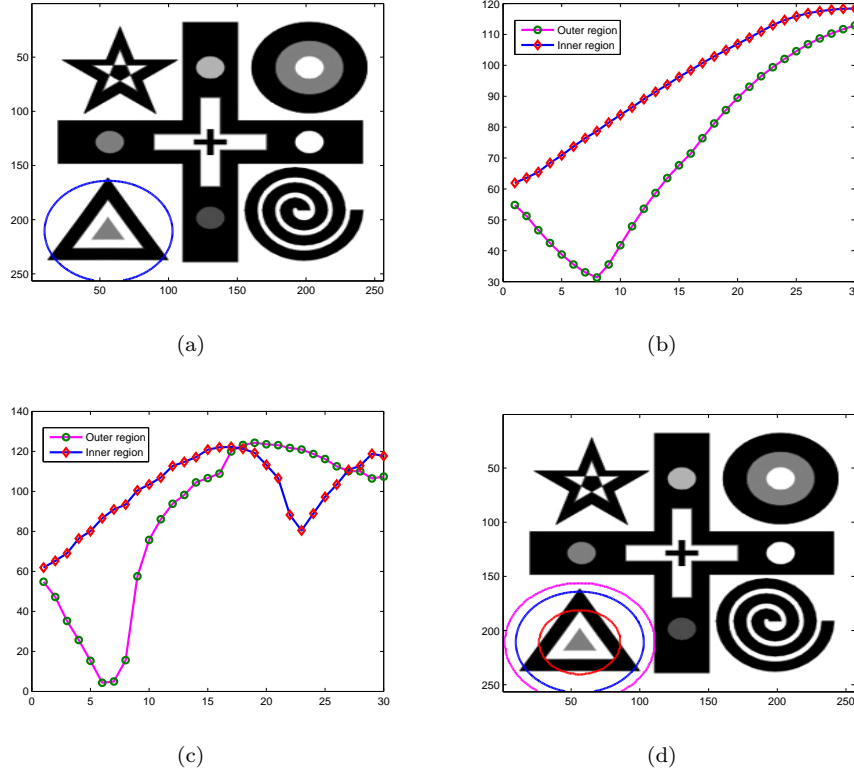


FIG. 3. Inner and outer γ -choice by Algorithm 3. (a) the tested zero level; (b) Mean variation $MIV_{in}(\gamma)$ and $MIV_{out}(\gamma)$ with respect to localizing parameter γ ; (c) Local mean variation $LMIV_{in}(\gamma)$ and $LMIV_{out}(\gamma)$ with respect to localizing parameter γ ; (d) Donuts with donut radiuses are localizing parameter $r = \gamma_{in} = 17$ and $r = \gamma_{out} = 8$ selected by Algorithm 3, respectively.

To illustrate our γ -choice by Algorithm 3, we consider one image with an initial guess (denoted by a large circle on the triangle shape) as shown in Fig.3(a) where we set $\gamma_{min} = 2, \gamma_{max} = 30$. Fig.3(b) shows the mean variation curves of $MIV_{in}(\gamma)$ and $MIV_{out}(\gamma)$ as defined by (19) and (21); one observes that $MIV_{in}(\gamma)$ is an increasing function with respect to γ so γ_{in} has to be decided by using $LMIV_{in}(\gamma)$. But $MIV_{out}(\gamma)$ has a clear extremal point and defines an optimal parameter $\gamma_{out} = 8$. Fig.3(c) shows the local mean variation curves of $LMIV_{in}(\gamma)$ and $LMIV_{out}(\gamma)$ by (20) and (3.2); our concerned $MIV_{in}(\gamma)$ curve has three extremal points $\gamma = 17, 23, 29$ so we take the optimal value $\gamma_{in} = 17$. The other curve $MIV_{out}(\gamma)$ is not needed but it shows two extremal points $\gamma = 6, 19$ (which would suggest $\gamma_{out} = 6$ if it is not yet decided). Thus on this initial optimization step, Fig.3(d) indicates that the optimal choices are $\gamma_{in} = 17, \gamma_{out} = 8$ by Algorithm 3. Further we found that $MI_{in} = 202.4, MI_{out} = 250.1, MGI_{in} = 9.8$ and $MGI_{out} = 4.3$ (i.e. gradient variations not small) so we do not need to reset $\gamma_{in} = 17, \gamma_{out} = 8$.

An explicit scheme for a gradient descent method for equations (15) and (18) is implemented in our numerical experiments. As with F-M, our V-M is also stopped if the maximum number of evolving iterations is reached (usually $it = 3000$), or the relative error in two consecutive iterative steps is smaller than a small number $\eta_0 > 0$ (typically $\eta_0 = 10^{-6}$ for a practical segmentation), or the total number of pixels of $\phi < 0$ is smaller than 10. A pseudo-code implementation of our V-M is then summarized in Algorithm 4.

Algorithm 4 (A Variable- γ Method based on local features(V-M)).

- step 1. Input markers set: $\mathcal{A} = \{\bar{x}^\ell = (x_1^\ell, \dots, x_m^\ell)^T : \ell = 1, \dots, \bar{\ell}\}$, $m = 2$ for 2D problem and $m = 3$ for 3D problem. Define γ_{max} , γ_{min} , and the initial level set function ϕ^0 . Let set $n = 0$ and $it = 2$.*
- step 2. Re-initialize the level set function ϕ^n by some algorithm (e.g. multigrid).*
- step 3. Obtain inner and outer band-width via Algorithm 2:*
 - $[\gamma_{in}^n, \gamma_{out}^n] = RLPCA(\gamma_{min}, \gamma_{max}, \eta_1, \eta_2, \eta_3)$;
- step 4. Update C_1, C_2 and then solve the evolving equation (18):*
 - $\phi^{n+1} = EL_VM_local(\phi^n, \gamma_{in}^n, \gamma_{out}^n, it)$;
- step 5. Check for convergence using the criteria as with F-M.*
 - *If not satisfied, set $n = n + 1$ and go to step 3;*
 - *Else return solution $\phi^* = \phi^{n+1}$.*

4. Numerical experiments. The main aim of this section is to show that our new Algorithm 4 is effective and robust in selectively segmenting the desired object boundary from different initial solutions and for synthetic and real medical images. In all experiments, a marker set $\mathcal{A} = \{x_i = (x_i^1, x_i^2) : i = 1, \dots, n_p\}$ is given around the boundary of the desired object, and the fitting weight $\lambda_1 = \lambda_2 = 1$ is fixed.

4.1. Refinements for the geometric constrained term. In this subsection, we briefly give the details on how to improve the performances of model by employing the geometric constrained term (other explains also refer to [8, 22]). Here we only explain how the markers distance function performs when a marker set is supplied, and see more details about the edge function in [14].

In Fig.4, we test the above markers distance functions $d_1(x)$ from (8), $d_2(x)$ from (9) and our improving distance function $d_3(x)$ which is essentially $d_1(x)$ with a fixed σ replaced by $\sigma = \bar{\sigma} = \max(\sigma_1, \sigma_0)$ and $\sigma_1 = \min_{1 \leq i < j \leq n_p} |x_i - x_j|$ (to allow flexible scaling). Here all test images are of size 512×512 and the black regions indicate that the edge function approaches to 0, the white regions denote their intensities close to 1, red circles show the location of the markers. Fig.4(b) shows the performance of $d_1(x)$ with $\sigma = 4$ like in [8, 22] where only very small regions are effected by the marker set and, furthermore if the initial zero level is given the location of outside of this region, its influence also will be lost; so the performance of this function in model also is negligible. We can also observe that $d_2(x)$ extends its influence in a much large region which unfortunately would encourage an evolving curve to reach other unintended objects. Our improving distance function $d_3(x)$ with automatically tuned parameter $\bar{\sigma}$ is shown in Fig.4(d) where a large but localised capturing region is found. So we recommend the improved $d_3(x)$ as the new distance function in our model.

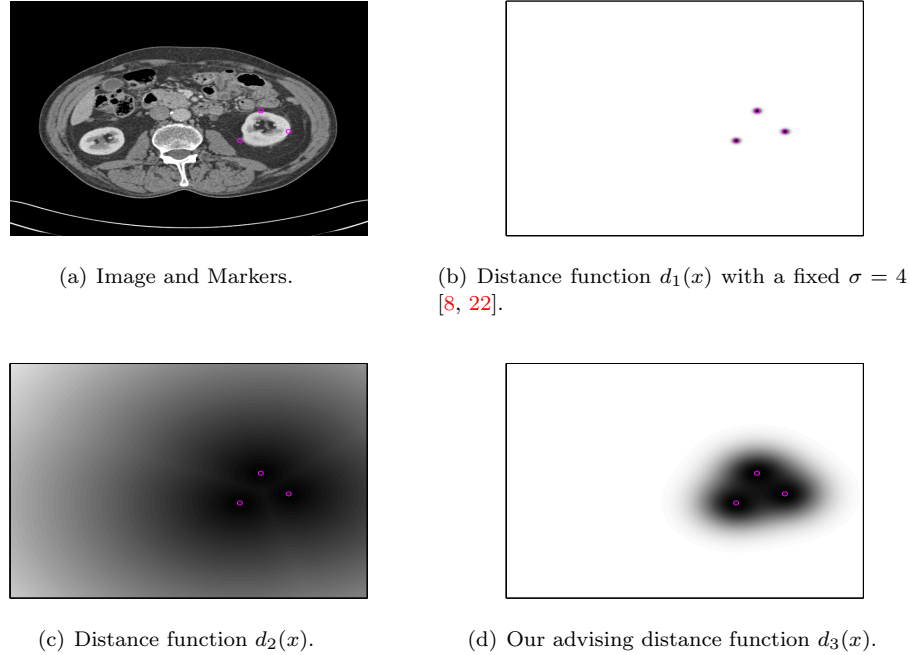


FIG. 4. Comparison of three distance functions

Clearly with the above choices for the markers distance function, the contour Γ is encouraged to evolve into the neighborhood of markers by optimizing $d(x)$ (especially when one reduced the weight of the local intensity fitting term), whereafter the edge function and the local intensity energy will play important roles in driving the contour Γ to the edge of object.

Before we test the proposed numerical algorithm, we first remark on how the markers influence the results; several examples in Fig.5 illustrate the efficiency of the locations of the markers for the selective segmentation problem. The successful cases include setting

- four markers within Γ in Fig.5(a);
- five markers around the edge Γ in Fig.5(b);
- five markers outside but near the edge Γ in Fig.5(c).

As somehow expected, the unsuccessful cases include setting

- six markers far away from Γ in 5(d);
- four markers to define an initialization covering both part of the intended object and another unintended object in Fig.5(e).

Although three markers provide a minimum set for our model to work, increasing the marker set would help fast and selective segmentation.

4.2. The tests for proposed fixed- and variable- γ methods. In this subsection, through experiments, we aim to

1. demonstrate the advantages of our V-M over the F-M in delivering a successful segmentation result for different regularization parameters α .

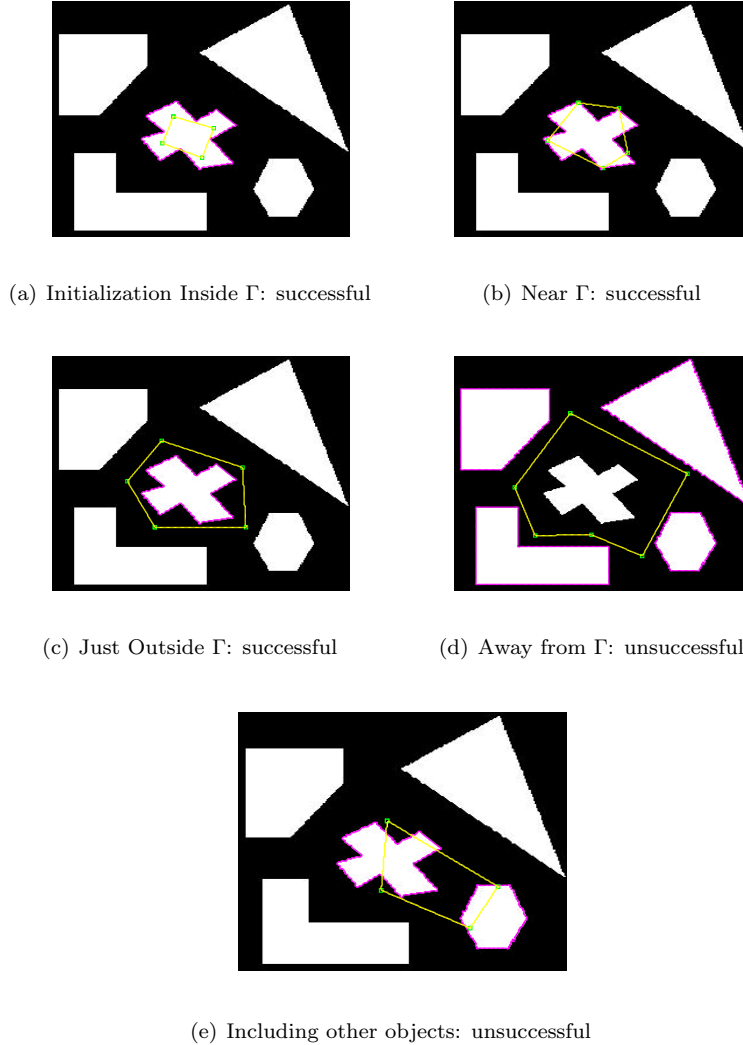


FIG. 5. Test on the influence of geometric marker sets and initialization on model performance.

2. compare the V-M with our F-M with a range of fixed parameters γ to conclude that there does not exist a robust choice.
3. show the advantages of the V-M over the F-M in selectively segmenting a noisy image.

Two test sets will be used in this subsection, to be named as Test1A, Test1B respectively as represented in Fig.6. For simplicity, below, we use the symbol “ \times ” to denote a failed segmentation result, “ w ” a result with redundant objects (also failed) and “ \checkmark ” a success.

4.2.1. *Dependence tests on the regularization parameter α .* The regularization parameter α in a global segmentation model not only controls a balance of the terms

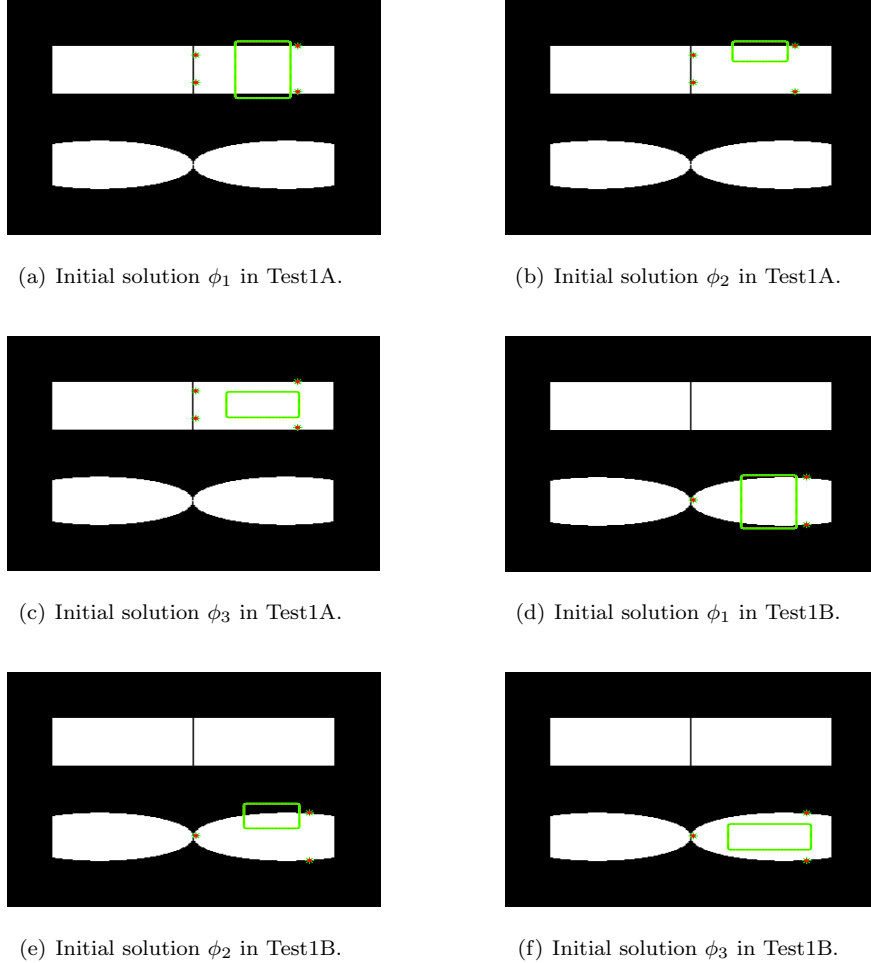


FIG. 6. Test datasets. Problem Test1A with three different initial guesses ϕ_1 , ϕ_2 and ϕ_3 followed by Problem Test1B with further three different initial guesses ϕ_1 , ϕ_2 and ϕ_3 from top/left to bottom/right, where red stars are markers constraining the target.

but also implicitly defines the minimal diameter of detected objects among a possibly noisy background. For (10), we investigate out variable- γ method and the fixed- γ method for different regularization parameters α . We take Test1A and Test1B as shown in Fig.6 to illustrate comparisons between two methods. We use $\alpha = 0.1 \times 255^2$, 0.01×255^2 .

Firstly we consider $\alpha = 0.1 \times 255^2$ for both methods: we test the F-M with a localizing parameter ranging from $\gamma = 2$ to $\gamma = 7$ and the V-M. The same initial guesses are used in both methods. Tab.1 summarizes the results for such tests. In Test1A with $\alpha = 0.1 \times 255^2$, if $\gamma = 2$ is used, the contour will shrink to one point as the curve evolves, but inversely if $\gamma = 7$ is chosen, the contour will pass through the thin edge and detect the nearest (redundant) objects. However, $\gamma = 3-6$ are

three feasible choices from our experiments. For the V-M, since γ is automatically selected, a successful segmentation is obtained. The results of Test1B are also represented in Tab.1 with similar observations. Secondly with the regularization parameter $\alpha = 0.01 \times 255^2$, we also show the results for both methods in the bottom row of Tab.1. As expected from the experiments, although both methods are very successful in segmenting the given images; less choices of γ for the F-M lead to successful segmentation.

α	Test1A-1							Test1B-1				
	F-M						V-M	F-M				V-M
	2	3	4	5	6	7		2	3	4	5	
0.1×255^2	✗	✓	✓	✓	✓	w	✓	✗	✓	✓	w	✓
0.01×255^2	✓	✓	w	w	w	w	✓	✓	w	w	w	✓

TAB. 1. Comparisons for the regularization parameter α -independence.

4.2.2. *Dependence tests on initial level set contours.* For tests Test1A and Test1B, three different initial guesses ϕ_1, ϕ_2 and ϕ_3 (as shown in Fig.6) are tested to assess the robustness of the proposed methods.

In Tab.2 we present the segmentation results from our tests. It appears that ϕ_3 cannot make the F-M work for any γ . In contrast, the V-M is successful for any initial guess.

To visualize the synthetic image (Test1A), we show in Figure 7 (a)-(c), the segmentation contours, where for completeness the first column of plots shows three initial positions for Test1A with four markers, the results from using the F-M with three different fixed parameters γ (middle 3 columns) and in the last column the result by the V-M. Here, one observes all three cases of symbols shown in Tab.2, where P=Problem. Clearly our V-M is robust.

3)

P	Test1A									Test1B									
Ini ϕ	ϕ_1			ϕ_2				ϕ_3			ϕ_1			ϕ_2			ϕ_3		
γ	2	3-6	7	4	5	6	7	23	24	25	2	3-4	5	4	5	22	23	24	
F-M	✗	✓	w	✗	✗	✓	w	✗	w	w	✗	✓	✗	✗	w	✗	w	w	
V-M	✓			✓				✓			✓			✓			✓		

TAB. 2. Comparisons of segmentation results from different initial guesses.

4.2.3. *The tests for noise images.* To assess the effect of noise on our models, we repeat the first two cases ϕ_1, ϕ_2 of Fig. 7 with noise added.

In Tab.3 and Fig.8, we have summarized the test results. One observes that while the F-M still works with the initial guess ϕ_1 and one particular choice of $\gamma = 6$, it fails in the other case. Clearly the V-M method works fine.

In summary, we observe that the F-M uses a fixed size of the inner and the outer narrow bands to restrict the evolution of the curve, in the other words, the V-M adjusts the size of the bands at each iteration automatically by Algorithm 3 to efficiently abstract regions of interest and to provide robustness. The results from the above comparisons show that the V-M out performs the F-M.

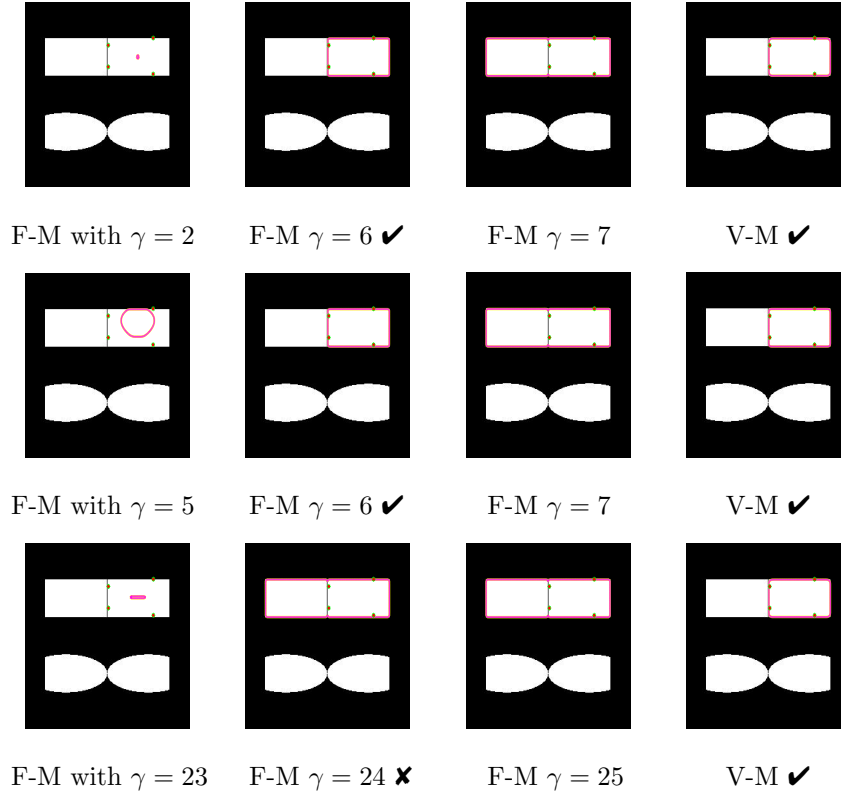


FIG. 7. Comparisons of F-M and V-M for different initial guesses of Test1A (Fig.6). From left to right in top line with ϕ_1 : Contour by F-M with $\gamma = 2$, $\gamma = 6$, $\gamma = 7$, contour by V-M; from left to right in middle line with ϕ_2 : Contour by F-M with $\gamma = 5$, $\gamma = 6$, $\gamma = 7$, contour by V-M; from left to right in bottom line with ϕ_3 : Contour by F-M with $\gamma = 23$, $\gamma = 24$, $\gamma = 25$, contour by V-M. Clearly the use of a fixed narrow band alone does not lead to a robust method.

Problem	Initial level set	γ	F-M	V-M
Test1A-Noise	ϕ_1	2	✗	
		3-6	✓	✓
		7	w	
	ϕ_2	4	✗	
		5-11	w	✓
		12	w	
	ϕ_3	22	✗	
		23	w	✓
		24	w	

TAB. 3. Comparisons for noisy images.

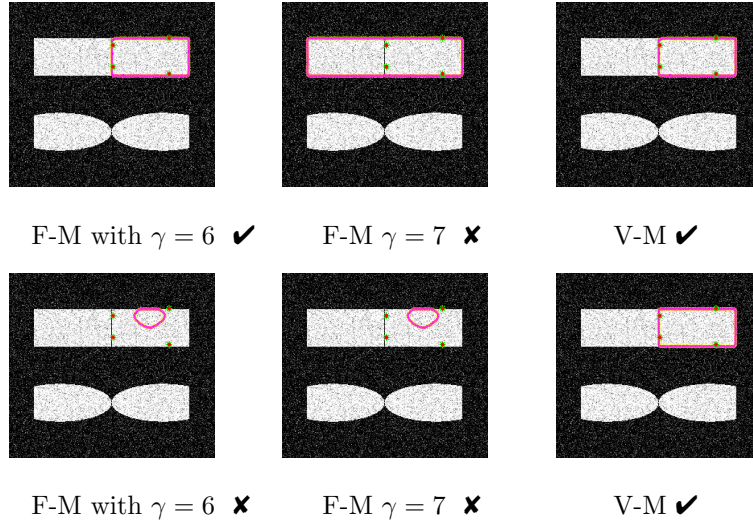


FIG. 8. Comparisons of F-M and V-M in dealing with noise images using the first two initial guesses of Test1A (Fig.6). From left to right in top line with ϕ_1 : Contour by F-M with $\gamma = 6$, $\gamma = 7$, contour by V-M; from left to right in top line with ϕ_2 : Contour by F-M with $\gamma = 6$, $\gamma = 7$, contour by V-M. Again V-M is better.

4.3. Comparison with global energy models. It is true that for simple examples where the desirable object is well separated from neighboring ones, one can even use a global segmentation model to selectively segment the object (because a localized level set function can get converged to a local solution). However, this does not lead to a reliable method and the necessity of a selective segmentation becomes apparent with realistic images.

Here for two examples, we compare the segmentation results of our V-M method with the Chan-Vese [18] model. Both methods start from the same initial curves. From Fig.9, one observes that the global model fails for the first example but it gives a reasonable segmentation for the second one (which would be classified as “w” as it picks up extra edges). In contrast, our V-M method delivers the desirable results.

4.4. Comparisons with the Badshah-Chen [8] model. We have explained that the Badshah-Chen [8] model has improved the geodesic model by Gout et al. [22] for noisy images, and that its gradient descent iterations can get close to the desirable solution but may pass it to converge to nearby (and redundant) objects if early termination is not done. Three test examples are given below.

Fig.10 shows the first comparative test for a medical MRI image; the original image with its initial zero level by a quadrilateral and 3 markers are shown in the top-left of Fig.10. We are interested in locating an organ on the right in the MRI image. We remark that many global segmentation methods are also tried and they all lead to incorrect results. The incorrect result obtained by using the Badshah-Chen model after 540 iterations contains the correct organ along with parts of other

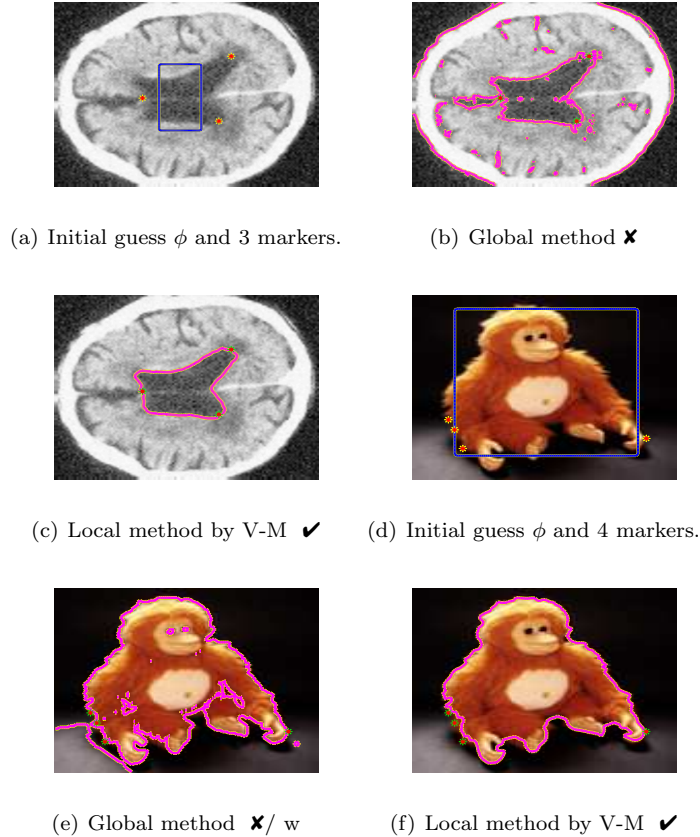


FIG. 9. Comparison of a global method with local initial guess and our local V-M. From left to right in top line: brain MRI image with 3 markers and initial zero level set, unsuccessful target detection by global, successful detection by V-M; From left to right in bottom line: monkey image with 4 markers and initial zero level set, unsuccessful detection, successful detection by V-M.

organs as shown in Fig.10 (b,d-e). In contrast, Fig.10 (c,f-g) show the correct result obtained by our V-M method.

The above test is repeated for two more examples respectively in Figs.11 and 12. In each case, (a) shows the initial contour along with geometric markers and plots (b,d-e) show the incorrect results by the Badshah-Chen model, while (c,f-g) show the correct result by by our V-M method.

4.5. Comparison with the Lankton model based on a local fitting energy.

We have remarked that there exist several models using a local fitting energy to localize a global segmentation model. Although our tests show that our adapted F-M model using a local fitting energy is not robust for selective segmentation, we wish to compare with other local models. The Lankton model [26] contains a localizing function, like our b function in (12) or (16), of local balls with varying sizes. To compare it with our V-M method, we consider both methods starting from

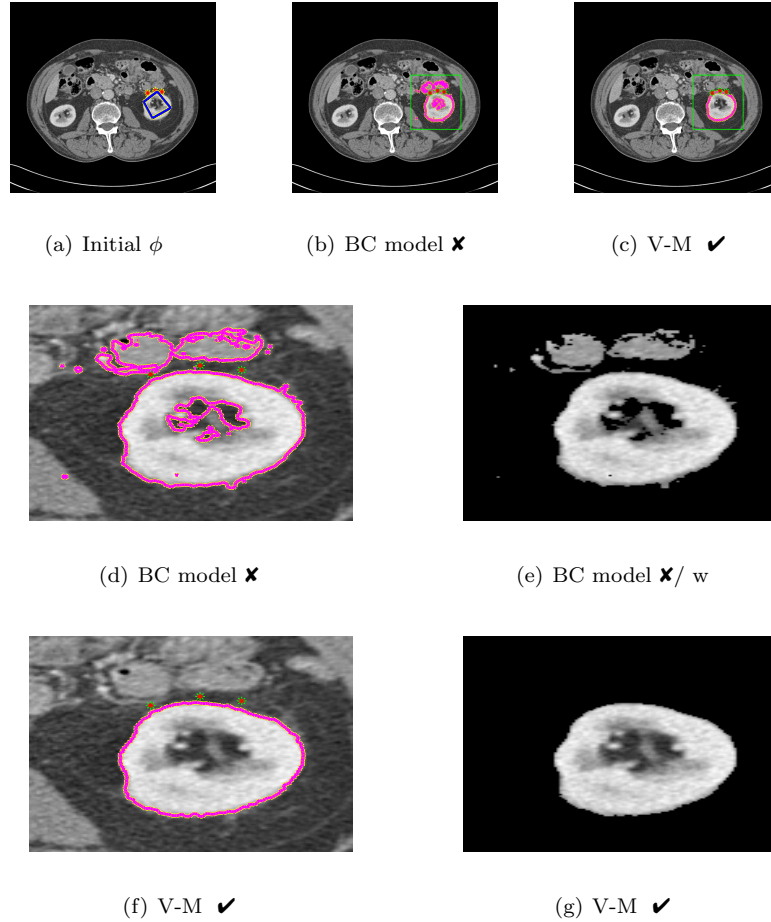


FIG. 10. Comparison 1 of the Badshah-Chen (BC) model and V-M. (a) Initial guess and 3 markers; (b) Unsuccessful result by the Badshah-Chen method; (c) Successful segmentation by V-M; (d) Close up representation of (b); (e) Unsuccessful result by the Badshah-Chen method; (f) Close up representation of (c); (g) Successful result by V-M.

two different initial contours as shown in Fig.13(a) and Fig.13(f) with 4 markers and the same $\alpha = 0.1 \times 255^2$. As before, column 1 of the plots shows the initial contours and the last column 5 shows the results from V-M, while the middle three columns showing results of the Lankton model after 15000 iterations with ball radii $r = 3$, $r = 9$ and $r = 13$ respectively. Clearly the Lankton model does not lead to redundant objects (unlike [8]) but fails to give the correct segmentation in the first case (middle 3 plots of row 1). It does succeed in the second case with (i) the ball radius of $r = 13$. In comparison, Fig.13 (e,j) show that our V-M method gives the correctly selected segmentation.

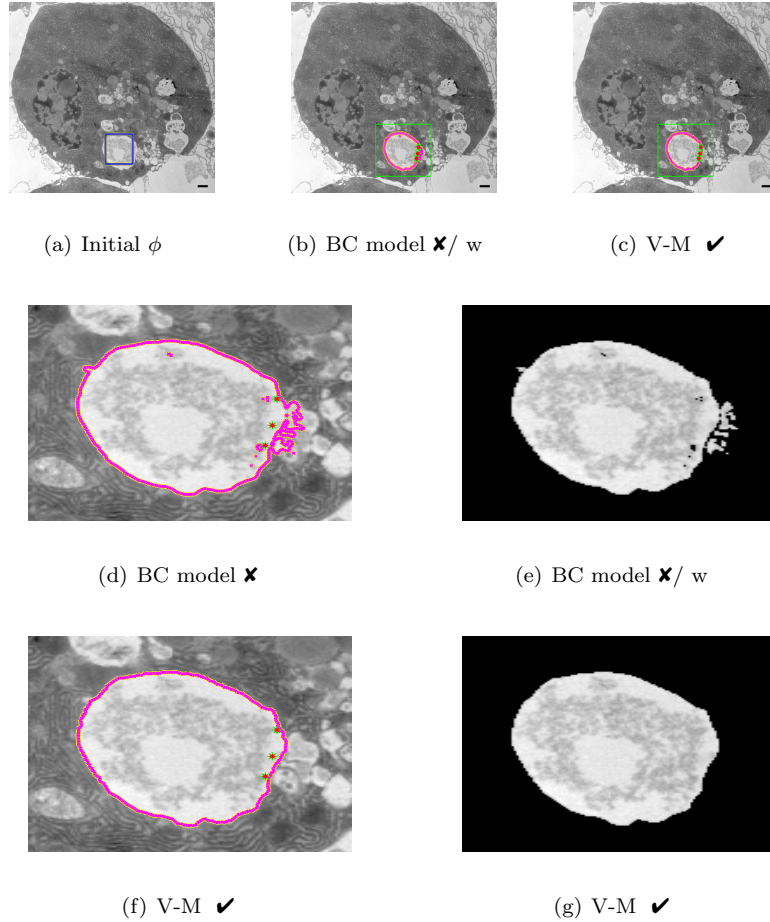


FIG. 11. Comparison 2 of the Badshah-Chen method and V-M. (a) Initial guess and 3 markers; (b) Unsuccessful result by the Badshah-Chen method; (c) Successful segmentation by V-M; (d) Close up representation of (b); (e) Unsuccessful result by the Badshah-Chen method; (f) Close up representation of (c); (g) Successful result by V-M.

5. Conclusions. In this paper we presented an efficient selective segmentation model based on the geometrical constraints (an edge detector function and a markers distance function) and the local features surrounding the evolving curve Γ , with an adaptively variable- γ band. Both F-M and V-M methods for capturing the local image intensity information around Γ are considered, with the latter recommended. Unlike previous work, our proposed methods do not need a ‘balloon’ force to drive the contour Γ to the edge of a desirable object. The numerical results indicated that our proposed method is fairly robust and reliable in terms of quality and robustness. On one hand it can segment selectively a single object with noise and complex structures and on the other hand it is less sensitive to initial solutions

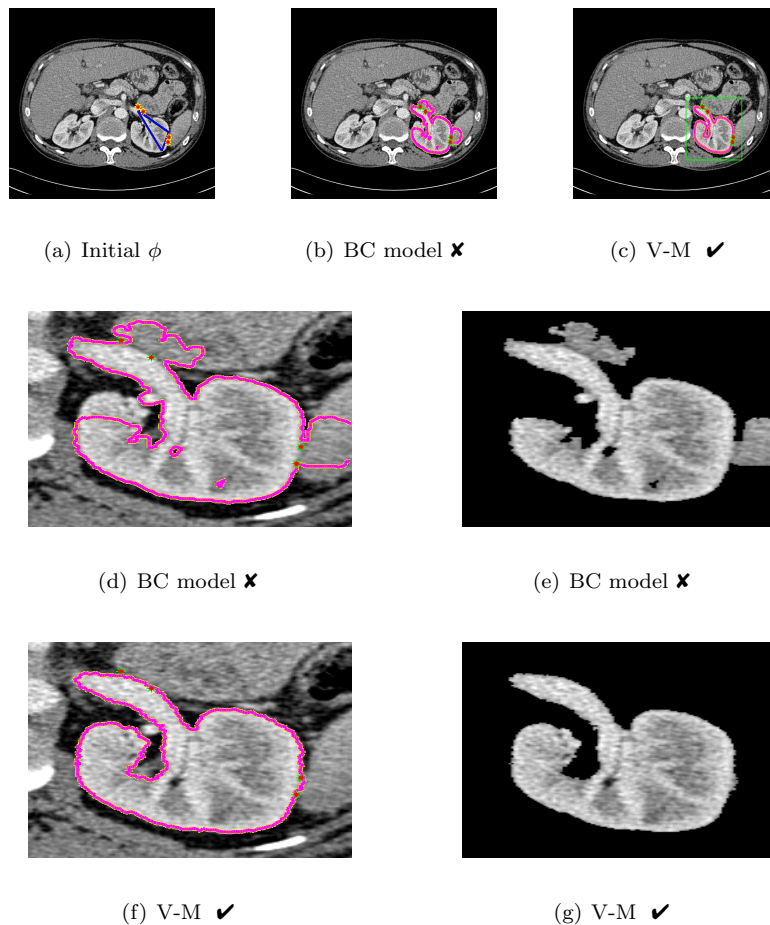


FIG. 12. Comparison 3 of the Badshah-Chen method and V-M. (a) Initial guess and 4 markers; (b) Unsuccessful result by the Badshah-Chen method; (c) Successful segmentation by V-M; (d) Close up representation of (b); (e) Unsuccessful result by the Badshah-Chen method; (f) Close up representation of (c); (g) Successful result by V-M.

than previous models. Future works will consider the local features based selective segmentation for texture images, and medical image selective segmentation in high dimensions.

Acknowledgments. The first author would like to thank the Research Centre for Mathematical Imaging Techniques (CMIT) and Royal Liverpool University Hospitals, UK for a supported visit to CMIT. The second author wishes to thank the School of Mathematical Sciences at DLUT for several invited visits.

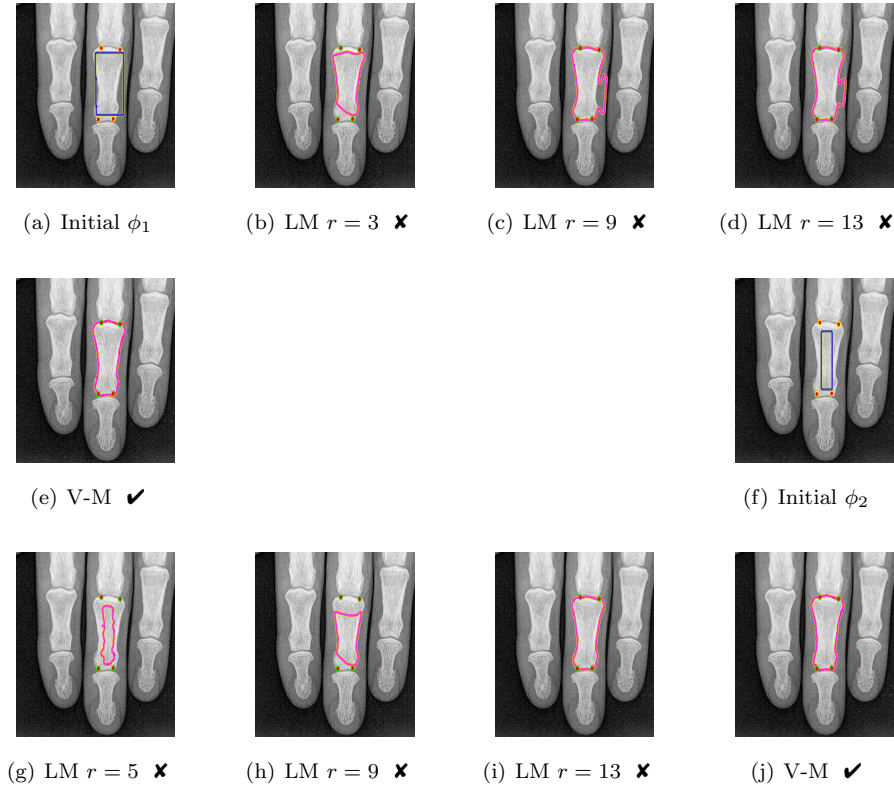


FIG. 13. Comparison of the Lankton model (LM) and our V-M. (a) Initial guess ϕ_1 and 4 markers; (b-d) Unsuccessful result by the LM with ball radii $r = 3$, $r = 9$ and $r = 13$, respectively; (e) Successful segmentation by V-M; (f) Initial guess ϕ_2 and 4 markers; (g-h) Unsuccessful result by the LM with ball radii $r = 5$ and $r = 9$, respectively; (i) Successful segmentation by the LM with ball radii $r = 13$; (j) Successful segmentation by V-M.

REFERENCES

- [1] D. Adalsteinsson and J. A. Sethian, [A fast level set method for propagating interfaces](#), *J. Comput. Phys.*, **118** (1995), 269–277.
- [2] D. Adalsteinsson and J. A. Sethian, [A level set approach to a unified model for etching, deposition, and lithography. II. Three-dimensional simulations](#), *J. Comput. Phys.*, **122** (1995), 348–366.
- [3] L. Ambrosio and V. Tortorelli, [Approximation of functionals depending on jumps by elliptic functionals via \$\Gamma\$ -convergence](#), *Comm. Pure and Applied Math.*, **43** (1990), 999–1036.
- [4] A. Araujo, S. Barbeiro and P. Serranho, [Stability of Finite Difference Schemes for Complex Diffusion Processes](#), Pre-print, Departamento de Matematica da Universidade de Coimbra, DMUC report 10-23, 2010.
- [5] G. Aubert and P. Kornprobst, *Mathematical Problems in Image Processing*, Springer, New York, 2002.
- [6] N. Badshah and K. Chen, [Multigrid method for the Chan-Vese model in variational segmentation](#), *Communications in Computational Physics*, **4** (2008), 294–316.

- [7] N. Badshah and K. Chen, [On two multigrid algorithms for modeling variation multiphase image segmentation](#), *IEEE Trans. Image Processing*, **18** (2009), 1097–1106.
- [8] N. Badshah and K. Chen, [Image selective segmentation under geometrical constraints using an active contour approach](#), *Commun. Comput. Phys.*, **7** (2010), 759–778.
- [9] X. Bresson, S. Esedoglu, P. Vanderghelynst, J. Thiran and S. Osher, [Fast global minimization of the active contour/snake models](#), *J. Math. Imaging and Vision*, **28** (2007), 151–167.
- [10] E. S. Brown, T. F. Chan and X. Bresson, [A convex approach for multi-phase piecewise constant Mumford-Shah image segmentation](#), *Int. J. Computer Vision*, **98** (2012), 103–121.
- [11] E. S. Brown, T. F. Chan and X. Bresson, [A convex relaxation method for a class of vector-valued minimization problems with applications to Mumford-Shah segmentation](#), UCLA CAM report 10-43, 2010.
- [12] M. Burger, G. Gilboa, S. Osher and J. Xu, [Nonlinear inverse scale space methods](#), *Commun. Math. Sci.*, **4** (2006), 179–212.
- [13] J. F. Canny, [Finding Edges and Lines in Images](#), Technical Report AITR-720, Massachusetts Institute of Technology, Artificial Intelligence Laboratory, 1983.
- [14] V. Caselles, R. Kimmel and G. Sapiro, [Geodesic active contours](#), *Int. J. Computer Vision*, **22** (1997), 61–79.
- [15] T. F. Chan, S. Esedoglu and M. Nikolova, [Algorithms for finding global minimizers of image segmentation and denoising models](#), *SIAM J. Applied Mathematics*, **66** (2006), 1632–1648.
- [16] T. F. Chan, B. Y. Sandberg and L. A. Vese, [Active contours without edges for vector-valued images](#), *J. Visual Commun. Image Representation*, **11** (2000), 130–141.
- [17] T. F. Chan and L. A. Vese, [An efficient variational multiphase motion for the Mumford-Shah segmentation model](#), *Proc. Asilomar Conf. Signals, Systems, Computers*, **1** (2000), 490–494.
- [18] T. F. Chan and L. Vese, [Active coutours without edges](#), *IEEE Trans. Image Processing*, **10** (2001), 266–277.
- [19] T. F. Chan and J. H. Shen, [Image Processing and Analysis: Variational, PDE, Wavelet and Stochastic Methods](#), SIAM, Philadelphia, 2005.
- [20] G. Gilboa, N. Sochen and Y. Zeeni, [Image enhancement and denoising by complex diffusion processes](#), *IEEE Trans Pattern Anal. Mach. Intell.*, **26** (2004), 1020–1036.
- [21] T. Goldstein, X. Bresson and S. Osher, [Geometric applications of the split Bregman method: Segmentation and surface reconstruction](#), *J. Sci. Computing*, **45** (2010), 272–293.
- [22] C. Gout, C. Le Guyader and L. A. Vese, [Segmentation under geometrical consitions with geodesic active contour and interpolation using level set methods](#), *Numerical Algorithms*, **39** (2005), 155–173.
- [23] C. Le Guyader, N. Forcadel and C. Gout, [Image segmentation using a generalized fast marching method](#), *Numerical Algorithms*, **48** (2008), 189–212.
- [24] M. Jeon, M. Alexander, W. Pedrycz and N. Pizzi, [Unsupervised hierarchical image segmentation with level set and additive operator splitting](#), *Pattern Recogn. Lett.*, **26** (2005), 1461–1469.
- [25] M. Kass, A. Witkin and D. Terzopoulos, [Snake: Active contour models](#), *Int. J. Computer Vision*, **1** (1988), 321–331.
- [26] S. Lankton and A. Tannenbaum, [Localizing region-based active contours](#), *IEEE Trans. Image Processing*, **17** (2008), 2029–2039.
- [27] C. Li, C. Kao, J. Gore and Z. Ding, [Implicit active contours driven by local binary fitting energy](#), *Proceedings of IEEE Conference on Computer Vision and Pattern Recognition (CVPR)* (Washington, DC, USA), *IEEE Computer Society*, (2007), 1–7.
- [28] F. Li, M. K. Ng and C. Li, [Variational fuzzy Mumford-Shah model for image segmentation](#), *SIAM J. Appl. Math.*, **70** (2010), 2750–2770.
- [29] J. Lie, M. Lysaker and X.-C. Tai, [A binary level set model and some applications to Mumford-Shah image segmentation](#), *IEEE Trans. Image Processing*, **15** (2006), 1171–1181.
- [30] R. Malladi, J. A. Sethian and B. C. Vemuri, [Shape modeling with front propagation: A level set approach](#), *IEEE Trans. Pattern Anal. Mach. Intell.*, **17** (1995), 158–175.
- [31] A. Marquina and S. Osher, [Explicit algorithms for a new time dependent model based on level set motion for nonlinear deblurring and noise removal](#), *SIAM J. Sci. Computing*, **22** (2000), 387–405.
- [32] H. Mewada and S. Patnaik, [Variable kernel based Chan-Vese model for image segmentation](#), *Annual IEEE India Conference (INDICON)*, (2009), 1–4.
- [33] J. Mille, [Narrow band region-based active contours and surfaces for 2D and 3D segmentation](#), *Computer Vision and Image Understanding*, **113** (2009), 946–965.

- [34] D. Mumford and J. Shah, [Optimal approximation by piecewise smooth functions and associated variational problem](#), *Commun. Pure Appl. Math.*, **42** (1989), 577–685.
- [35] S. Osher and R. Fedkiw, *Level Set Methods and Dynamic Implicit Surfaces*, Springer Verlag, 2005.
- [36] S. Osher and J. Sethian, [Fronts propagating with curvature dependent speed: algorithms based on Hamilton-Jacobi formulations](#), *J. Comput. Phys.*, **79** (1988), 12–49.
- [37] D. P. Peng, B. Merriman, S. Osher, H. K. Zhao and M. Kang, [A PDE-Based fast local level set method](#), *J. Comput. Phys.*, **155** (1999), 410–438.
- [38] J. M. S. Prewitt, Object enhancement and extraction, in *Picture Processing and Psychopictorics*, (eds. B. S. Lipkin and A. Rosenfeld), New York: Academic, (1970), 75–149.
- [39] J. A. Sethian, [Fast marching methods](#), *SIAM Review*, **41** (1999), 199–235.
- [40] J. H. Shen, [\$\Gamma\$ -Convergence approximation to piecewise constant Mumford-Shah segmentation](#), *Advanced Concepts for Intelligent Vision Systems*, **3708** (2005), 499–506.
- [41] I. Sobel, An isotropic 3×3 image gradient operator, *Machine Vision for Three-Dimension Scenes*, (ed. H. Freeman), (1990), 376–379.
- [42] M. Sussman, P. Smereka and S. Osher, [A level set approach for computing solutions to incompressible two-phase flow](#), *J. Comput. Phys.*, **114** (1994), 146–159.
- [43] X. C. Tai, O. Christiansen, P. Lin and I. Skjaelaaen, [Image segmentation using some piecewise constant level set methods with MBO type of projection](#), *Int. J. Computer Vision*, **73** (2007), 61–76.
- [44] L. A. Vese and T. F. Chan, A multiphase level set framework for image segmentation using the Mumford and Shah model, *Int. J. Computer Vision*, **50** (2002), 271–293.
- [45] H. K. Zhao, T. F. Chan, B. Merriman and S. Osher, [A variational level set approach to multiphase motion](#), *J. Comput. Phys.*, **127** (1996), 179–195.

Received July 2011; revised November 2012.

E-mail address: jpzhang@xtu.edu.cn

E-mail address: k.chen@liv.ac.uk (for correspondence)

E-mail address: yubo@dlut.edu.cn

E-mail address: Derek.Gould@rlbuht.nhs.uk